Structural, electrical, and optoelectrical characterization of PbS nanoparticles

ANJAN KUMAR MISHRA*, SATYAJIT SAHA
Department of Physics, Vidyasagar University, PaschimMidnapur, Pin-721102, West Bengal, India

Lead sulfide (PbS) nanoparticles show the potential to establish as photoelectrical materials for photodetectors for the next generation. The excellent electrical and optical properties including polarity, carrier mobility, carrier concentration, and conductivity are widely investigated using thin films of PbS nanoparticles and it is ascribed to the strong quantum confinement effects. The various optoelectronic devices are fabricated with PbS nanoparticles as versatile building blocks. The transport properties of thin films of these PbS nanoparticles depend on the size, shape, and stoichiometry. In the present study, chains like PbS, spherical PbS, and cubic PbS nanoparticles are grown by a cost-effective chemical reduction route. The effect of the quantity of reducing agents ($NaBH_4$) was investigated on the morphology and size of the products. Transmission Electron Microscopy (TEM) and X-Ray Diffraction (XRD) patterns show the formation of PbS nanoparticles. The average particle size is 8 nm, 15 nm, and 23 nm for Spherical, Cubic, and Chain PbS nanoparticles. EDS analysis also confirms the XRD results. Quantum confinement is achieved for different shaped PbS nanoparticles and hence thereby the bandgap is increased. The electrical parameter like conductivity, hole concentration, and hole mobility is determined from conductivity and Hall experiment data. Photoconductivity for all PbS samples was performed at room temperature under the illumination of 50 mW/cm^2. Photosensitivity and Detectiviy are calculated for different shaped PbS nanoparticles.

(Received November 11, 2020; accepted June 7, 2022)

Keywords: Lead sulfide, Nanomaterials, NIR-spectroscopy, Structural characterization, Electric characterization, Photoconductivity

1. Introduction

Recently, a semiconducting nanoscale material is mostly driven by the fabrication of novel electronic nanodevices and nanocircuits for their unique properties which are manipulated by their chemical environment, surface morphology, and also physical dimensions without trouble. The distributions of the particle molecules of ordered ensembles play a vital role in the variable electronic properties of the total assemblies. The synthesis of semiconducting nanoparticles has increased rapidly in recent times due to unique properties like restricted agglomeration and fine particle size distribution under the space confinement effect. Semiconducting nanoparticles are shown as encouraged the development of green energy and environmental remediation due to the utilization of SunPower and catalysts which are cost-effective [1-4]. Semiconducting nanoparticles show attractive applications for optoelectronic devices due to their more tunning optical properties with their solution processability. The sensitive photodetectors are designed by various methods using vacuum and expensive instruments. These devices also show a narrow detection range and responsivity due to inefficient carrier transfer. Lead sulfide has huge potential applications in high-efficiency optoelectronic. [5-8]. PbS nanostructures have properties like photoconductivity [9–12], photovoltaics [13], mechanical [14], photocatalytic [15], gas sensing [16].This device's quality depends on crystal defects, shape, size, surface properties, and phase by changing their preparation parameter and methods. There are so many methods to grow PbS nanostructures such as solvothermal [17], chemical deposition [18], thermal decomposition, hydrothermal [19], microwave [20], and sol-gel [21].PbS nanoparticle's intra-gap states originate due to an off-stoichiometry Pb-rich surface [22] or due to a charge imbalance between Pb atoms and capping ligands [23]. The electrical properties of PbS nanoparticles also depend on the formation of lead sulfates at the surface of nanoparticles after air exposure. The Charge-carrier capture coefficient is about 400 times higher for electrons in the case of these p-dopant agents and trapping centers [24]. Also for increasing the minority carrier lifetime due to traps PbS nanostructures can be applied in solar cells or light-emitting diodes [25]. E. M. Nasir et al. [26] observed the increases in positive photoconductivity in the prepared lead sulphide films. They showed photocurrent increases from 82 μA to 110 μA with increasing thickness of films. The photoconductivity is increased due to an increase in the grain size. They found photoconductive gain (G) which was the ratio between the photocurrent to the dark current at the same bias voltage. Its value was about 102.5 for 300 μm film thickness and 72.2 for film thickness 400μm at the same bias voltage of 15V. DhavalVankhade et al. [27] investigated the electrical and photo-electrical properties of PbS thin films deposited by the spin-coating technique. The PbS films were p-type and photoconductive. Electrical conductivity (σ) varied from 0.028 S/cm for the 250 nm film to 0.234 S/cm for the 500 nm film, while the hole concentration (p) value was the order of 10^{18} cm^{-3}, and mobility (μ) value was 0.5 - 5.8 cm^2/Vs of the films under illumination at room temperature. Photoconductivity was explained based on the trapping of minority carriers by sensitization centers. The mobility of holes (μ_L) of PbS films also increased under illumination. A.A. Ibrahim et al.

[28] prepared lead sulfide (PbS) thin films by thermal evaporation of PbS powder onto glass substrates. They found electron concentration (n_o) of ≈ (3.9 – 5.4) x 10^9 m^{-3} at room temperature. The derived value of permittivity was 5.3 x 10^{-11} Fm^{-1} (ε_r = 5.7) and there was necessary to assume a plausible value of μ = 6 x 10^{-6} m^2/Vs [29]. PbS nanoparticles are grown by a simple low-cost one-pot chemical method using ethylenediamine as a capping agent. The thin films of PbS nanoparticles are used to measure their electrical properties. The Hall experiment is done for fabricated films based on three different shaped PbS nanoparticles. PbS nanoparticles-based photodetectors are fabricated. Photosensitivity, Detectivity, and photoconductive sensitivity are measured for three different shaped PbS nanoparticles.

2. Experimental section

2.1. Chemicals and reagents

All chemicals, with high-class purity and analytical grade, were used to synthesize PbS nanoparticles. The reagents lead Chloride ($PbCl_2$), sulfur powder (S), sodium borohydride ($NaBH_4$), and ethylene-diamine were purchased from Sigma-Aldrich and were employed without further purification.

2.2. Synthesis of PbS nanoparticles

$NaBH_4$, anhydrous $PbCl_2$, and S powder are used as reagents and Ethelyn Diamine is used as a capping agent to synthesize PbS nanoparticles. At first, an amount of 2.78 g $PbCl_2$ was taken in 50 ml of EDA to three different beakers. This solution was stirred vigorously by using a magnetic stirrer. After half an hour, 0.32 g of sulfur was added to the above solution. Finally, 0.37 g, 1.11 g, and 1.85 g of $NaBH_4$ were added to three different beakers respectively to get grown PbS samples of different ratios as 1:1:1, 1:1:3, and 1:1:5 respectively. The solution was stirred at 1000 RPM using a magnetic stirrer for 4 hours. Then the solution was turned a black color. This indicated the formation of PbS nanoparticles. The residue product of grown samples was filtered, washed, and centrifuged. Finally, it was kept for two weeks in a clean dry place at room temperature.

2.3. Experimental method

High-resolution Rigaku Mini Flex X-ray Diffractometer is used to obtain X-ray diffraction (XRD) patterns of powder PbS samples. JEOL-JEM 2100 HRTEM is also used to get a TEM picture of PbS samples. SAED pattern is obtained from selected area electron diffraction. Scanning Electron Microscopy (SEM) pattern is taken for PbS samples. Agilent Technologies Cary 5000 Series UV-VIS-NIR Spectrophotometer is used to get absorption spectra of PbS samples after ultrasonication PbS samples in an ethanol medium. For electrical characterization, three different size PbS nanoparticle samples are deposited on clean glass by a spin coating technique. Also, electrical contacts of silver were painted for three different PbS films. Voltage and current in the circuit were measured by Keithley 4200 scs electrical parameter analyzer.

3. Results and discussions

3.1. Structural characterization

The morphology and particle size of grown PbS nanoparticles were investigated by TEM and SEM measurements. It is possible to obtain fine and homogenous PbS nanoparticles due to ultrasonication.

The time and power of ultrasonication play a vital role in the purity of PbS nanoparticles. PbS nanosamples are sonicated in ethanol for 30 minutes with a power of 40 watts to prepare the TEM grid.

TEM images of different PbS Nanoparticles are shown in Fig. 1.

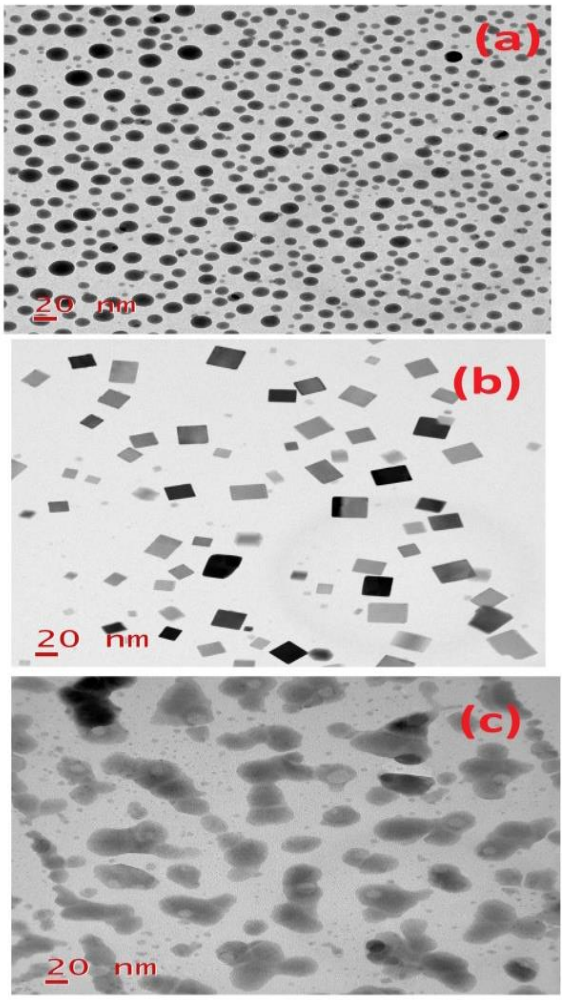

Fig. 1. The TEM images of (a) Spherical PbS (b) Cubic PbS NPs (c) Chain-like PbS(color online)

The spherical shape PbS nanoparticles were seen from the TEM picture for reagents ratio of 1:1:1, cubical shape for the ratio of 1:1:3, whereas chain-like PbS for the ratio of 1:1:5.The particle size of PbS nanoparticles increases

with an increase in the reagent ratio. From the TEM picture particle size of Spherical PbS, Cubic PbS NPs, and Chain-like PbS were calculated as 8 nm, 15 nm, and 23 nm respectively.

The SEM images of different PbS Nanoparticles are shown in Fig. 2.

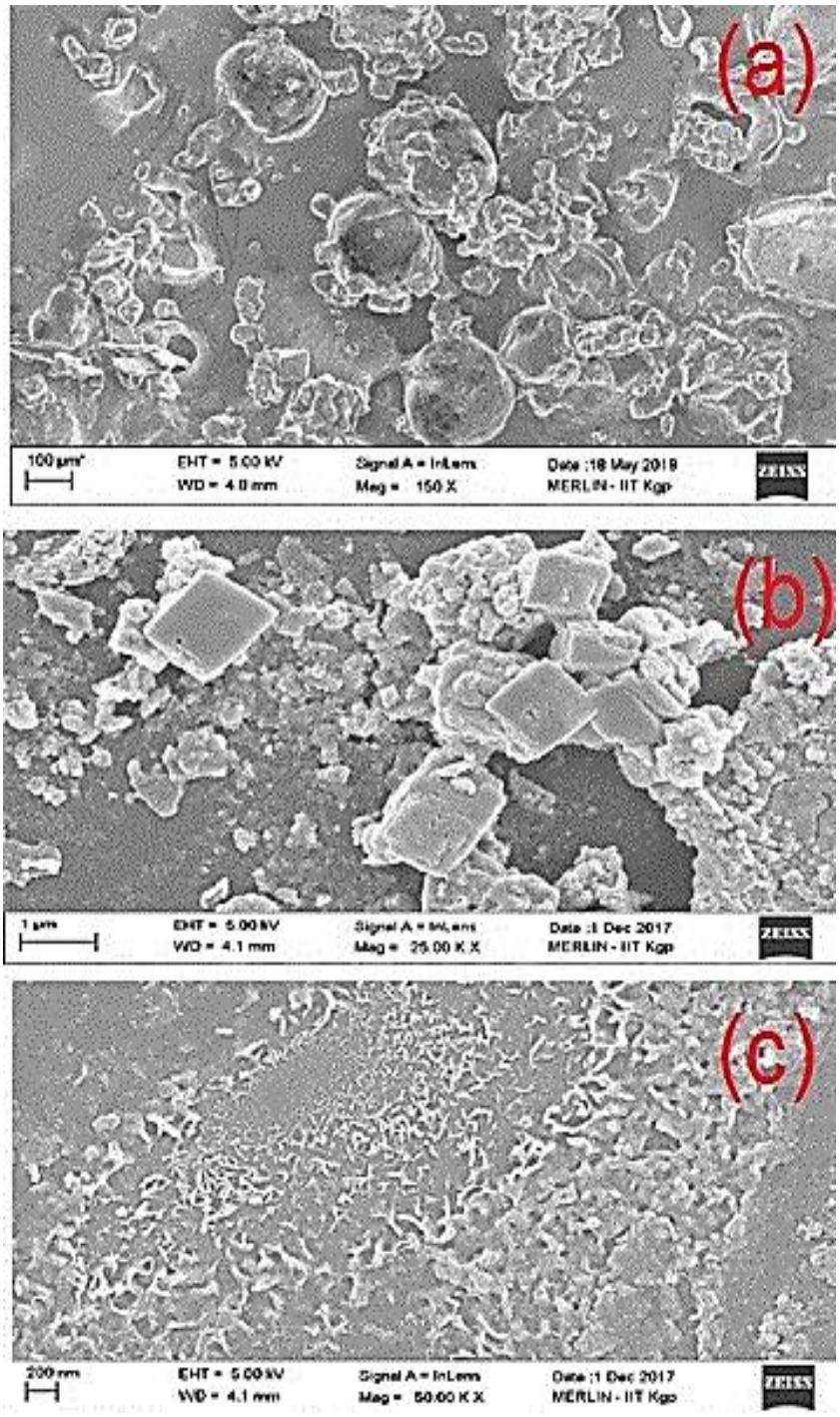

Fig. 2 The SEM images of (a) Spherical PbS (b) Cubic PbS NPs (c) Chain-like PbS (color online)

SEM micrograph shows the film surface consists of a granular structure with grains in Chain-like PbS. We also see clusters on the film surface and large particles extend beyond the surfaces of the Chain like PbS. This is clear from the figure that all the prepared PbS nanoparticles are at nanometer ranges. The morphology of PbS nanoparticles of 1:1:3 ratio is small in dimensions in the cubical form of clusters. Whereas 1:1:1 ratio PbS nanoparticles show different morphology with smaller dimensions and the size clusters with spherical structures. Also, SEM micrographs are seen as rather dense and non-uniform.

The EDX spectra of different PbS Nanoparticles are shown in Fig 3.

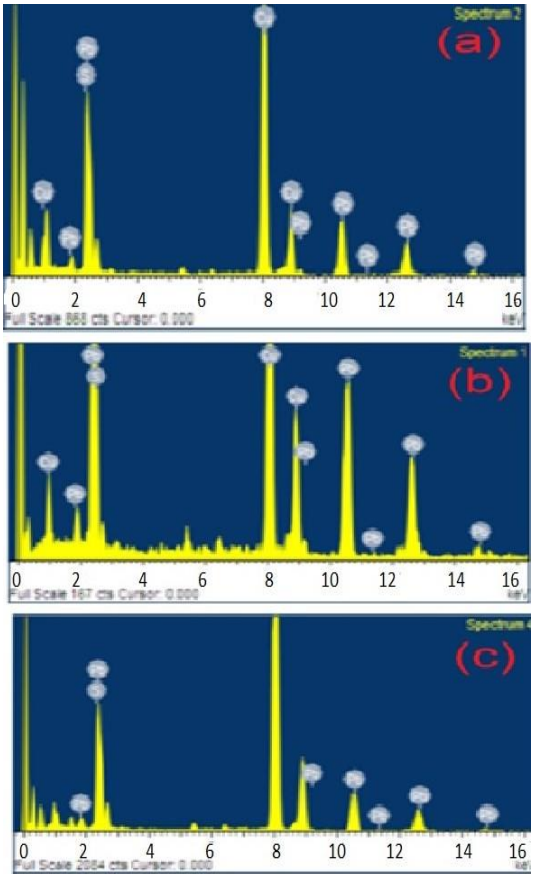

Fig. 3 The EDX patterns of (a) Spherical PbS (b) Cubic PbS NPs (c) Chain-like PbS (color online)

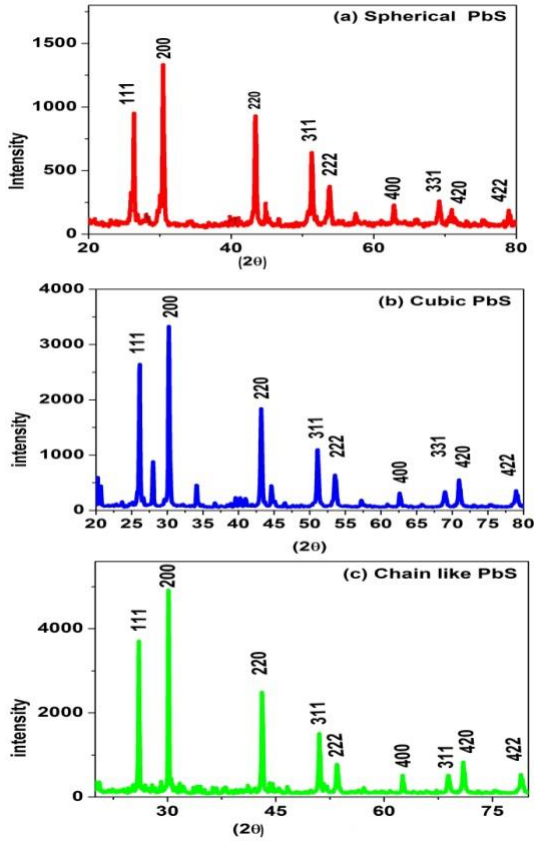

Fig. 4. XRD patterns of (a) Spherical PbS (b) Cubic PbS NPs (c) Chain-like PbS (color online)

The EDX pattern shows the presence of Pb and S elements in the chemical composition of the nano sample. This observation correlates with the XRD results and also supports this result. The EDX analysis proves the composition of the nano samples. XRD patterns of different PbS Nanoparticles are shown in Fig. 4.

X-Ray Diffraction (XRD) patterns of different shapes PbS nanoparticles are shown. XRD pattern is obtained with Cu-Kα x-rays of wavelength 1.5418 A^0. The lattice constant ($a = b = c$) is calculated from XRD data is 5.9 A^0. From the XRD pattern, we confirm the crystalline structure, phase purity, and average distribution of the size of the particles. From the XRD pattern, it was observed that most of the X-ray diffraction peaks for the different PbS Nanoparticles confirm the polycrystalline nature of PbS samples. PbS samples were face-centered cubic structures. The diffraction peaks at the different Bragg's angle (2θ) values are corresponding to (111), (200), (220), (311), (222), (400), (331), (420) and (422) planes respectively. X-ray diffraction peak broadening may be due to compressive strain for the difference in radii of particles. Nanocrystal size can be estimated using the Debye–Scherrer equation [30] which is given by

$$D = \frac{k}{b \cos\theta} \ ,$$

where D is crystal diameter, k is a shape constant value of 0.94 here, λ is the x-ray wavelength (1.5405 Å), b is the full width at half-maximum (FWHM) of the diffraction line, and θ is the diffraction angle in radian. The average particle size calculated from the XRD pattern was nearly equal to the particle size calculated from its TEM picture.

We calculate the texture coefficient (TC(*hkl*)) [31] from XRD data to show the different crystalline planes with the degree of preferred orientation. The relation is given below.

$$TC(hkl) = \frac{\frac{I(hkl)}{I_{card}(hkl)}}{\frac{1}{n}\sum_n \left[\frac{I(hkl)}{I_{card}(hkl)}\right]}$$

where I_{card}(hkl) is the intensity from PDF card number 04-003-2980 reference pattern and where is the intensity of the XRD pattern of PbS nanoparticles and bulk PbS and n is the number of diffraction peaks identified. For TC(*hkl*) of less than 1 or equal to1 shows that the distribution of powder material is random for each crystallographic plane. For values of TC(*hkl*) greater than 1 show the oriented planes.TC(*hkl*) value is determined using XRD data for two different shapes PbS nanoparticles and bulk PbS are given in Table 1. For the highest TC(*hkl*) value it implies that the plane (400) is more oriented in three different shaped PbS nanoparticles.

Table 1. X-ray diffraction intensities and preferred orientation factor for PbS nanoparticles

h	k	l	I_{xrd}			I_{card}	Texture Coefficient (TC(*hkl*))		
			Spherical PbS	Cubic PbS	Chain like PbS		Spherical PbS	Cubic PbS	Chain like PbS
1	1	1	976	2484	3766	913	0.68258	0.98072	1.04692
2	0	0	1343	3325	4901	999	0.85628	1.19975	1.24515
2	2	0	944	1681	2600	679	0.88553	0.89241	0.97187
3	1	1	628	1053	1633	396	1.01011	0.95852	1.04663
2	2	2	376	588	1084	217	1.10365	0.97675	0.98833
4	0	0	233	362	380	92	1.61314	1.41836	1.28007
3	3	1	267	342	464	133	1.27868	0.92695	1.06866
4	2	0	248	544	560	229	0.68979	0.85631	0.3724
4	2	2	216	342	603	156	0.88193	0.79026	0.98106

3.2. Optical characterization

The optical absorption spectra of different PbS nanoparticles are shown in Fig. 5.

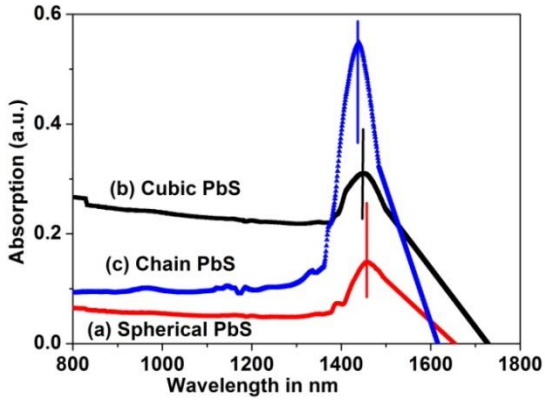

Fig. 5. The absorption spectra of (a) Spherical PbS (b) Cubic PbS NPs (c) Chain-like PbS (color online)

The thickness of the film based on PbS nanoparticles was measured by 3D - Optical Surface Profilometer. Whereas thickness value of the film was 0.071 µm,0.082 µm, and 0.095 µm for spherical PbS, cubic PbS nanoparticles, and Chains like PbS respectively. The optical absorption coefficient (α) is calculated with wavelength variation to determine the optical band gap of PbS nanoparticles. We used the Tauc method following the relation [32] $(\alpha h\gamma)^2 = \text{Const}(h\gamma - E_g)$ for PbS Nanoparticles. Bandgap (E_g) of PbS is determined by extrapolating the tangent of $(\alpha h\gamma)^2$ vs. hɣ plot. Spherical and cubical-shaped PbS nanoparticles have bandgap energy of 1.01 eV, 0.94 eV respectively, while the Chain-like PbS bandgap 0.89 eV. This bandgap is ascribed to the quantum confinement effect due to the smaller size of the PbS nanoparticles. We see the absorption maxima shifted towards the higher energy region for smaller size particles.

The bandgap calculation plots of different PbS nanoparticles are shown in Fig. 6.

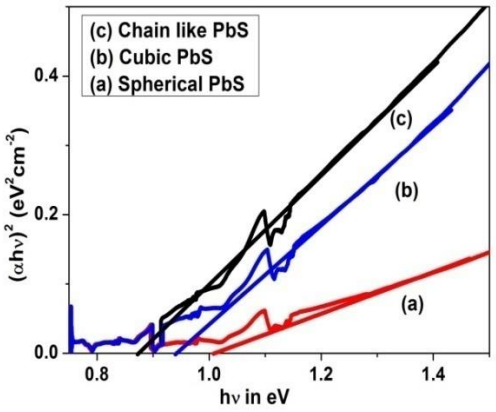

Fig. 6. Bandgap calculation plots for (a) Spherical PbS (b) Cubic PbS (c) Chain-like PbS (color online)

3.3. Electrical characterization

The Hall-effect experiments were done at a constant current (1 nA) with the magnetic field of 0.277 Tesla at Room Temperature using the Vander Pauw 4 probe electrical Measurement technique via the contacts of spring action four gold pins. The carrier concentration, resistivity, conductivity, and mobility of the PbS samples were derived from Hall-effect measurement. Hall coefficient is obtained positive for PbS samples by confirming a p-type charge carrier.PbS thin films based on spherical PbS nanoparticles show the electron mobility of 7.96×10^{-3} $m^2V^{-1}s^{-1}$ .The electrical parameters of PbS samples are given in Table.M. F. Afsar et al showed the density of states of PbS nanosheets was in the order of 10^{32} eV^{-1} cm^{-3}. They showed the electrical conductivity in the order of 10^{-3} Sm^{-1} at 300 K [33].

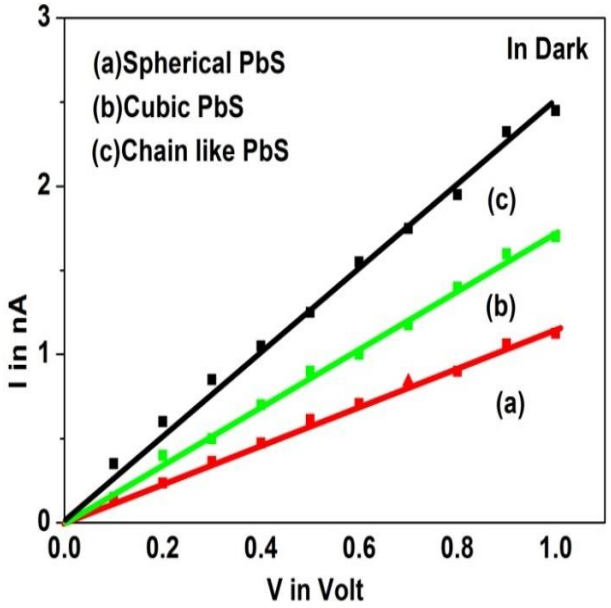

Fig. 7. The plot of Current vs voltage in dark at room temperature of different PbS nanoparticles photoconductors (color online)

The temperature variation of σ_T for different PbS Nanoparticles is shown in Fig. 8.

The Arrhenius equation [33] is given by $\sigma_T=\sigma_0 \exp(-E_a/KT)$ where E_a is the activation energy, T is the temperature in Kelvin, K is the Boltzmann constant and σ_0 is the pre-exponential factor. Photoexcitation and distance between nanoparticles also play a vital role in the electrical conductivity of PbS samples. H. Tang et al [34] showed the conductivity value [1.2×10^{-6} (S cm^{-1})] of the fabricated PbS films.We plot $\log\sigma_T$ along Y-axis and 1000/T along the X-axis, from the slope we calculate E_a.

The final results are shown in Table. We have calculated E_a for different PbS nanoparticles. It is seen that conductivity increases but mobility decreases slightly as particle size increases. Activation energy decreases with an increase in particle size.

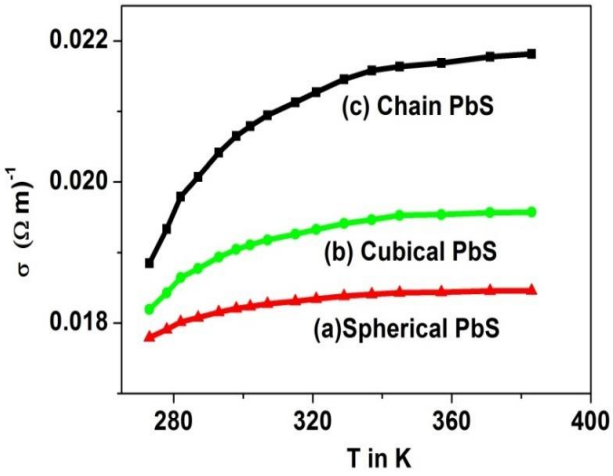

Fig. 8. The plot of Conductivity vs temperature of different PbS nanoparticles photoconductors (color online)

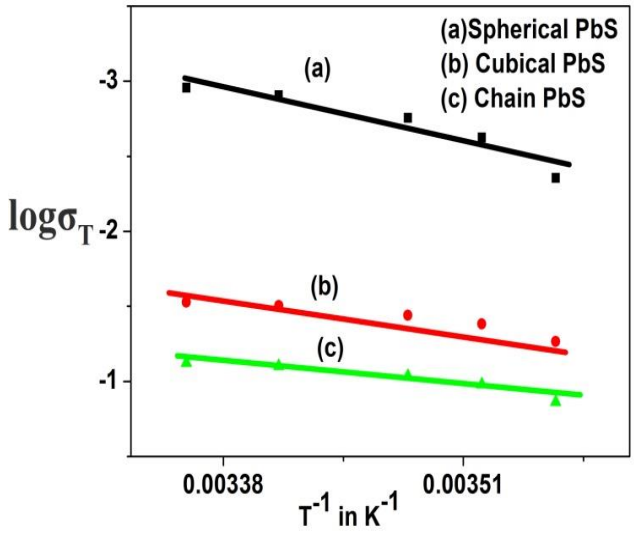

Fig. 9. The Plot of $\log\sigma_T$ as a function of 1/T for (a) Spherical PbS (b) Cubic PbS NPs (c) Chain-like PbS (color online)

Hole concentration, Mobility, Conductivity, Resistivity, Activation Energy of three different shaped PbS nanoparticles are given in Table 2.

Table 2. Hole concentration, Mobility, Conductivity, Resistivity, and Activation Energy of different PbS nanoparticles

PbS NPs (Shape, Size)	Hole Concentration (p) in m^{-3}	Mobility (μ) $\times 10^3$ in $m^2V^{-1}S^{-1}$	Conductivity (σ) in (Ω m)$^{-1}$	Resistivity (ρ)in (Ωm)	Activation Energy (E_a) in eV
Spherical, 8 nm	1.49×10^{19}	7.96	0.019	52.6	0.34
Cubical , 15nm	1.76×10^{19}	7.93	0.021	47.6	0.21
Chain like, 23nm	1.87×10^{19}	7.91	0.024	41.6	0.14

3.4. Photoconductive characterization

Change of photocurrent with time under 50mW/cm^2 illumination intensity and light off condition of different PbS nanoparticles photodetectors are shown in Fig 10.

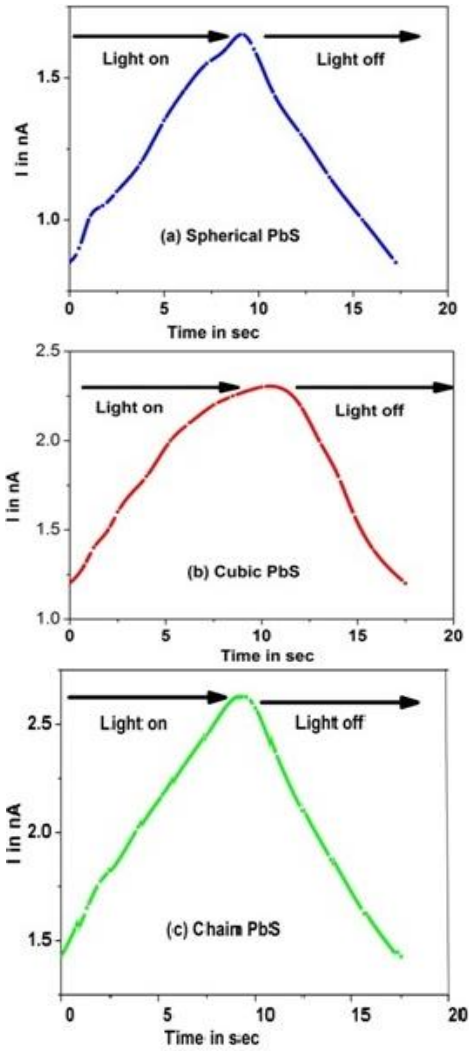

Fig. 10. The plot of current with time under 50mW/cm^2 illumination intensity and light off condition of (a) Spherical PbS (b) Cubic PbS NPs (c) Chain-like PbS (color online)

Photosensitivity and responsivity are the main two key factors for a good photodetector. The photodetector works depending on the synthesis condition and properties of PbS nanoparticles. The nanoPbS thin films are p-type conducting and introduced acceptor (traps) states on the film surface due to the oxidation [35-38]. The EDX analysis shows the result of stoichiometry that these states may originate due to the Pb-rich surface region of PbS films. These trap states in p-type semiconducting materials lie close to the conduction band edge so there is a high probability of thermal excitation back of the trapped charge carriers into the conduction band. Those bands of states lie close to the middle of the bandgap so the trapped charge carriers have a high probability of recombination due to photoexcitation via the hopping process [39-42]. Electrons in the PbS samples are excited from the valence band to the conduction band by absorbing a photon. Photo-generated holes in the valence band may transfer by hopping in nanocrystals. The Photo-response of the device is enhanced by the plasmonic effect. Current-voltage data of fabricated photoconductors are taken in dark conditions and also under light illumination. The linear and symmetrical graph of the dark current is due to the good ohmic contact of silver. Dark resistance and dark current density of PbS samples are in the order of GΩ and 10 mA/cm^2 respectively for 1 volt biasing voltage. Photosensitivity (PS) of the PbS samples is given by PS=(R_d-R_{ph})/R_{ph} where R_d is the electrical resistance in dark conditions and R_{ph} stands for the electrical resistance of the detector under illumination. As we used the same voltage using ohm law the photosensitivity (PS) of a detector is modified to PS=(I_{ph}-I_d)/I_d where the dark current is I_d and photocurrent is I_{ph} of the detector. Responsivity is defined as a ratio of the photocurrent to the incident optical power. For current sensing operation mode in a photodetector, Responsivity (R) is the amount of output current (i_{out}) per watt of input power (p_{in}). Its unit is A/W. It is given as follows. $R_i(\lambda, f) = \frac{i_{out}}{p_{in}}$The Responsivity value, which was derived by Y. Wei et al [43] was about 830 mA/W for the organic /PbS QD device. Quantum efficiency (QE) is defined as follows

Q. E. = $\frac{R_{observed}}{R_{ideal}}$ = R$\frac{hc}{\lambda q}$= 1.24×10^3×$\frac{R}{\lambda}$ The percentage of the incident photons that contribute to the photocurrent is called the Quantum efficiency. It is given above where R is the Responsivity in A/W, h is the Planck constant, c is the velocity of light, q is the charge of the electron, and λ is the wavelength in nm. It is expressed as a percentage. PbS samples made photoconductors show large responsivity. We also calculate Detectivity (D) of detector made from PbS samples by this formula D = $R_\lambda\sqrt{(A/2e\ I_d)}$where $R_\lambda$is the responsivity at the wavelength of λ (550 nm), A is the effective area of the photoconductor (A = a× b, where aand bare the channel length and width, 70 nm and 0.5cm, respectively), and e is the absolute value of electron charge. The Detectivity values for Spherical PbS nanoparticles were found, 7×10^{10} Jones. The Detectivity value of fabricated photodetector devices based on PbS nanoparticles was shown by Y. Wang et al. [44] in the range of 1.4×10^{11} Jones at 635 nm. E. Heves et al fabricated photodetectors based on PbS QDs and derived 0.667 A/W responsivity, 53.3% quantum efficiency, and also detectivity 2.12×10^{10} Jones under the condition of 3 V reverse bias and 5 mW/cm^2 illumination intensity at 1550 nm [45].

Dark conductivity, Photoconductivity, Detectivity, and Photoconductive Sensitivity of three different shaped PbS nanoparticles are given in Table 3.

Table 3. Dark conductivity, Photoconductivity, Detectivity, and Photoconductive Sensitivity of different PbS nanoparticles

Sample	Dark conductivity (σ_0)in (μS/m)	Photoconductivity ($\Delta\sigma$) in (μS/m)	Responsivity in A/W	Detectivity in (Jones)	Quantum efficiency (%)	Photoconductive Sensitivity $[(I_L-I_D)/I_D]\times100\%$
Spherical PbS	0.019	0.037	0.80	7×10^{10}	45	74
Cubic PbS	0.020	0.039	0.77	6.3×10^{10}	43	69
Chain like PbS	0.021	0.040	0.76	5.8×10^{10}	41	65

4. Conclusions

In this work different sizes and shaped PbS nanoparticles are grown by chemical reduction route in a cost-effective way. The films of grown Spherical PbS NPs, Cubic PbS NPs, and Chain-like PbS nanoparticles are characterized to investigate the effect of size and shape on electrical parameters. The result shows the grown spherical PbS nanoparticles are smaller in size compared to other shapes. As a result, the spherical PbS NPs show higher photoresponse compared to other shape nanoparticles Spherical shape PbS NPs show a higher photoconductive sensitivity, Responsivity, Detectivity, and Quantum efficiency compared to other two different shape nanoparticles due to higher quantum confinement.These results are evident from the tables given above. The relation between shape, size, and electrical as well as optoelectrical properties of PbS nanoparticles are very important for the development of cost-effective photodetector and quantum dot solar cells.

Acknowledgements

The authors are grateful to UGC & DST for their constant support through SAP and the FIST program to the Department of Physics.

References

[1] F. Ansari, A. Sobhani, M. Salavati-Niasari, Journal of Colloid and Interface Science **514**, 723 (2018).
[2] A. Salehabadi, M. Salavati-Niasari, M. Ghiyasiyan-Arani, Journal of Alloys and Compounds **745**, 789 (2018).
[3] Y. Orooji, M. Ghanbari, O. Amiri, M. Salavati-Niasari, Journal of Hazardous Materials **389**, 122079 (2020).
[4] A. E. Oluwalana, P. A. Ajibade, Optical and Quantum Electronics **53**, 2 (2021).
[5] S. Krishna, Journal of Physics D: Applied Physics **38**(13), 2142 (2005).
[6] S. Hoogland, V. Sukhovatkin, H. Shukla, J. Clifford, L. Levina, E. H. Sargent, Optics Express **16**(9), 6683 (2008).
[7] H. D. Jahromi, M. H. Sheikhi, M. H. Yousefi, Optics & Laser Technology **44**(3), 572 (2012).
[8] H. D. Jahromi, M. Sheikhi, M. Yousefi, Optics & Laser Technology **43**(6), 1020 (2011).
[9] S. McDonald, P. Cyr, L. Levina, E. Sargent, Applied physics letters **85**(11), 2089 (2004).
[10] G. Konstantatos et al., Nature **442**(7099), 180 (2006).
[11] A. D. Stiff-Roberts, K. R. Lantz, R. Pate, Journal of Physics D: Applied Physics **42**(23), 234004 (2009).
[12] H. D. Jahromi, M. H. Sheikhi, IEEE Sensors Journal **16**(6), 1634 (2016).
[13] G. Taher, S. Farimand, J. Choi, Microelectronic Engineering **183**, 48 (2017).
[14] A. Bueno, I. Suárez, R. Abargues, S. Sales, J. P. M. Pastor, IEEE Sensors Journal **12**(10), 3069 (2012).
[15] S. Coe, W. K. Woo, M. Bawendi, V. Bulovic, Nature **420**(6917), 800 (2002).
[16] T. Fu, Sensors Actuators, B Chem **140**, 116 (2009).
[17] P. Zhao, J. Wang, G. Cheng, K. Huang, The Journal of Physical Chemistry B **110** (45), 22400 (2006).
[18] E. Pentia, L. Pintilie, I. Matei, T. Botila, E. Ozbay, J. Optoelectron. Adv. M. **3**(2), 525 (2001).
[19] R. H. Yin, Q. S. Wu, Y. Chen, Chemical Papers **61**, 224 (2007).
[20] D. Liang, S. Tang, J. Liu, J. Liu, X. Lv, L. Kang, Materials Letters **62**, 2426 (2008).
[21] M. S. Bakshi, P. Thakur, S. Sachar, Gurpreet Kaur, Tarlok Singh Banipal, Fred Possmayer, Nils O. Petersen, The Journal of Physical Chemistry C **111**, (49), 18087 (2007).
[22] H. Cao, Q. Gong, X. Qian, H. Wang, J. Zai, Z. Zhu, Crystal Growth &Design **7**(2), 425 (2007).
[23] R. Wang, Y. Shang, P. Kanjanaboos, W. Zhou, Z. Ning, E. H. Sargent. Energy & Environmental Science **9**(4), 1130 (2016).
[24] F. Pelayo García de Arquer, F. J. Beck, M. Bernechea, G. Konstantatos, Applied Physics Letters **100**(4), 043101 (2012).
[25] Y. Shirasaki, G. J. Supran, M. G. Bawendi, V. Bulović, Nature Photonics **7**(1), 13 (2013).
[26] E. M. Nasir, M. M. Abass, Chalcogenide Letters **16**(8), 409 (2019).
[27] D. Vankhade, T. K. Chaudhuri,J. Appl. Phys. **127**, 175107 (2020).
[28] A. A. Ibrahim, Defect and Diffusion Forum **294**, 85 (2009).
[29] R. Jin, G. Chen, and J. Pei, J. Phys. Chem. C **116**,

16207 (2012).
[30] A. K. Mishra, S. Saha,Chalcogenide Letters **17**(3), 147 (2020).
[31] S. Rex Rosario, I. Kulandaisamy, A. M. S. Arulanantham, K. Deva Arun Kumar, S. Valanarasu, Mohd Shkir, A. Kathalingam, S. AlFaify, Mater. Res. Express. **6**, 056416, (2019).
[32] A. K. Mishra, S. Saha, Int. J. Electrochem.Sci. **15**, 11594 (2020).
[33] M. F. Afsar, Arifa Jamil, and M. A. Rafiq, Adv. Nat. Sci.: Nanosci. Nanotechnol. **8**, 045010 (2017).
[34] H. Tang, J. Zhong ,W. Chen, K. Shi, G. Mei, Y. Zhang, Z. Wen, P. Müller-Buschbaum, D. Wu**,** K. Wang**,** X. W. Sun, ACS Appl. Nano Mater **2**(10), 6135 (2019).
[35] D. Vankhade, T. K. Chaudhuri, AIP Conference Proceedings **1942**,060001 (2018).
[36] S. Munde, N. Shinde, P. Khanzode, M. Budrukkar, P. Lahane, J. Dadge, S. Jejurikar, M. Mahabole, R. Khairnar, K. Bogle, Material Research Express **5**, 066203 (2018).
[45] E. Heves, Y. Gurbuz, IEEE Sensors Journal **14**(3), 816 (2014).
[37] Y. Pei, R. Pei, X. Liang, Y. Wang, L. Liu, H. Chen, J. Liang, Scientific Reports **6**, 21551 (2016).
[38] D. Kim, D-H Kim, J. H. Lee, J. C. Grossman, Physical Review Letters **110**,196802 (2013).
[39] A. K. Rath, M. Bernechea, L. Martinez, G. Konstantatos, Advanced Materials **23**, 3712 (2011).
[40] R. H. Bube, Photoconductivity of Solids, Wiley, 1960.
[41] R. Saran, R. J. Curry, Nature Photonics **10**, 81 (2016).
[42] J. Gao, J. M. Luther, O. E. Semonin, R. J. Ellingson, A. J. Nozik, M. C. Beard, Nano Letters **11**, 1002 (2011).
[43] Y. Wei, Z. Ren, A. Zhang, P. Mao, H. Li, X. Zhong, W. Li, S. Yang, J. H. Wang, Adv. Funct. Mater. **28**(11), 1706690 (2018).
[44] Y. Wang, Z. Liu, N. Huo, F. Li, M. Gu, X. Ling, Y. Zhang, K. Lu, L. Han, H. Fang, A. G. Shulga, Y. Xue, S. Zhou, F. Yang, X. Tang, J. Zheng, M. A. Loi, G. Konstantatos, W. Ma, Nature Communications **10**, 5136 (2019).

Corresponding author: anjanmishra2011@gmail.com